1

Climate and Environmental Modelling Programme (CEMP)

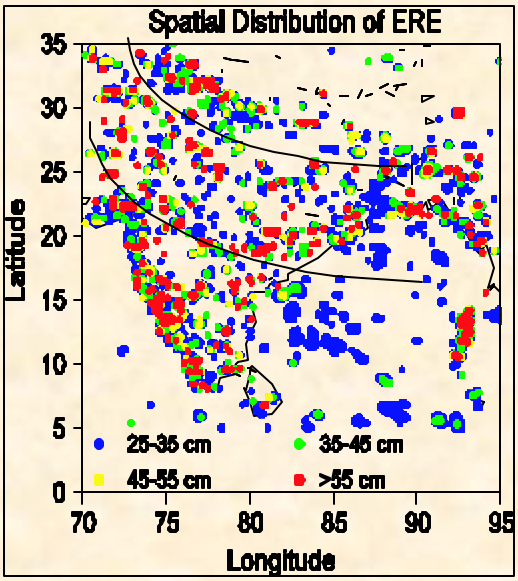

Inside

1.1 Experimental Long-range, High-Resolution Forecast of Monsoon Rainfall: Post-Forecast Evaluation

Predictability and forecast skill are complex functions of scale, process and model configuration. In particular, it is not clear what the basic skill in forecasting monsoon rainfall at high-resolution and long-range is. At the same time, only forecasts with high spatial resolution can meet the user needs, it is important to explore and quantify the skill at such forecasts objectively. As a part of its sustained effort to develop capability for long-range, high-resolution dynamical forecast of monsoon rainfall, and to build up statistics of skill for such forecasts, C-MMACS has been generating experimental forecasts since 2003. These experimental forecasts are thus generated for the sole purpose of objective, transparent post-forecast evaluation of forecast skill. The forecast model is a variable-resolution GCM adopted from a version developed at Laboratory for Dynamic Meteorology (LMD), France. A special feature of the model is that it allows selectively high resolution (zoom) over a given area (such as the Indian summer Monsoon region), thus allowing high-resolution simulation of monsoon at a relatively affordable computational cost. For improved forecast skill, however, the model must also be supplemented with appropriate forecast methodology. C-MMACS uses a Multi-grid Ensemble (MuGE) methodology, specially developed for long-range monsoon forecasting.

As forecast of actual rainfall is difficult due to still unavoidable model bias, forecasts are often made for anomalies, which are the departures from the corresponding long-period mean. Thus while the observed anomalies are derived with respect to observed climatology, the forecast anomalies are computed with respect to the model climatology. The C-MMACS (anomaly) forecasts are based on a 25-year model climatology. With this philosophy, experimental long-range, high-resolution forecast of monsoon rainfall was generated for 2006.

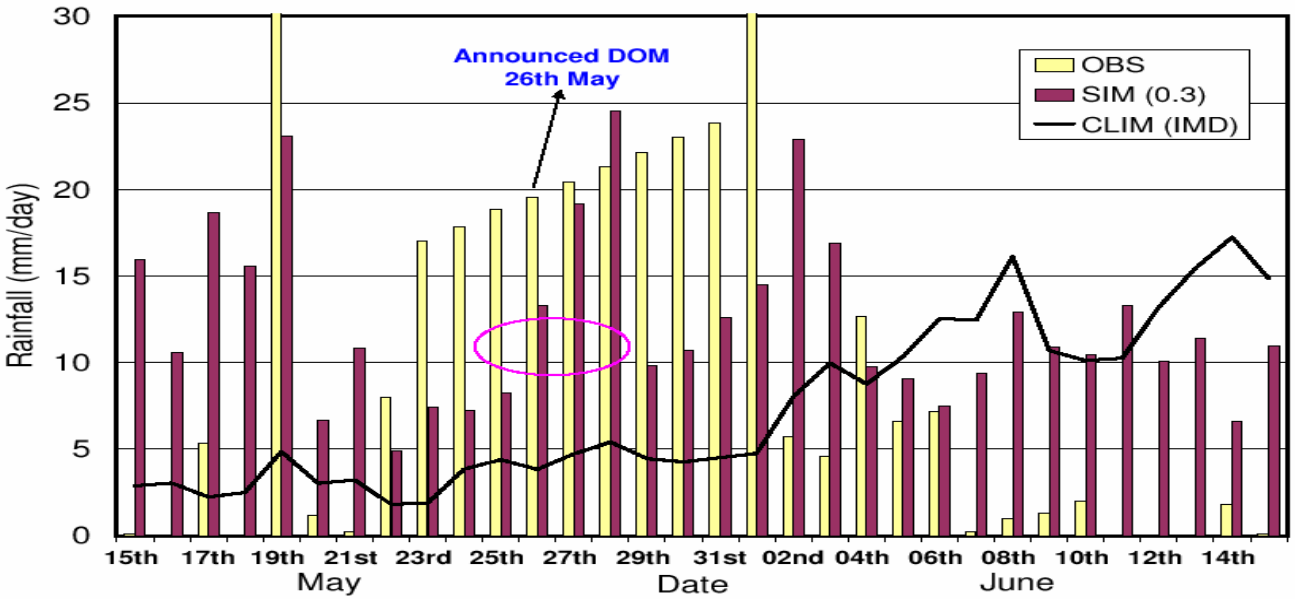

Figure 1.1 Area-averaged (75-77E; 8-12N) daily rainfall from nine-member ensemble forecasts for the period May 15 to June 15, 2006. The encircled days (May 25 to May 28) mark the first episode of large-scale, sustained and significant rain over the coast of Kerala and the onset of monsoon 2006 according to our definition. The correlation coefficient between observed and simulated daily rainfall is 0.3.

As mentioned above, one basic objective of C-MMACS experimental forecasts is to explore achievable skill at different scales with improved forecast configuration. We have therefore explored the model's skill in capturing the onset of monsoon rainfall. It is obvious that a unique definition of onset does not (and cannot) exist, as the definition depends on the emphasis. With our focus on rainfall and the users, we have defined the onset of monsoon as the day in May/June period on which rainfall occurs with the following characteristics:

(a) Large-scale: should occur more or less simultaneously over a number of stations.
(b) Significant: should be above a threshold value, typically 3 mm/day.
(c) Persistent: should last a few days with characteristics intermittently (day-to-day-variation).
(d) Sustained: The first spell should be followed by another rainfall spell with a gap of no more than 10 days.

While the criteria (a)-(c) have been advocated by others, the criteria (d) is our addition; its implementation requires forecasts for days subsequent to onset.

With this definition, the onset date for 2006 is predicted as May 26, based on an ensemble of 9 simulations based on initial conditions during the period 09 February to 25 March, 2006.

The forecasts of monthly anomalies are made by first calculating anomalies with respect to 25-year model mean for each member of the ensemble. The ensemble average is then determined as average over the ensemble with equal weight. The monthly rainfall anomaly, normalized to the 25-year climatology, for the month of June is presented in Figure 1.2 below (left panel), where the anomalies are expressed as percentage of model mean, it also compares the monthly rainfall anomaly for June from C-MMACS forecast with the IMD observation.

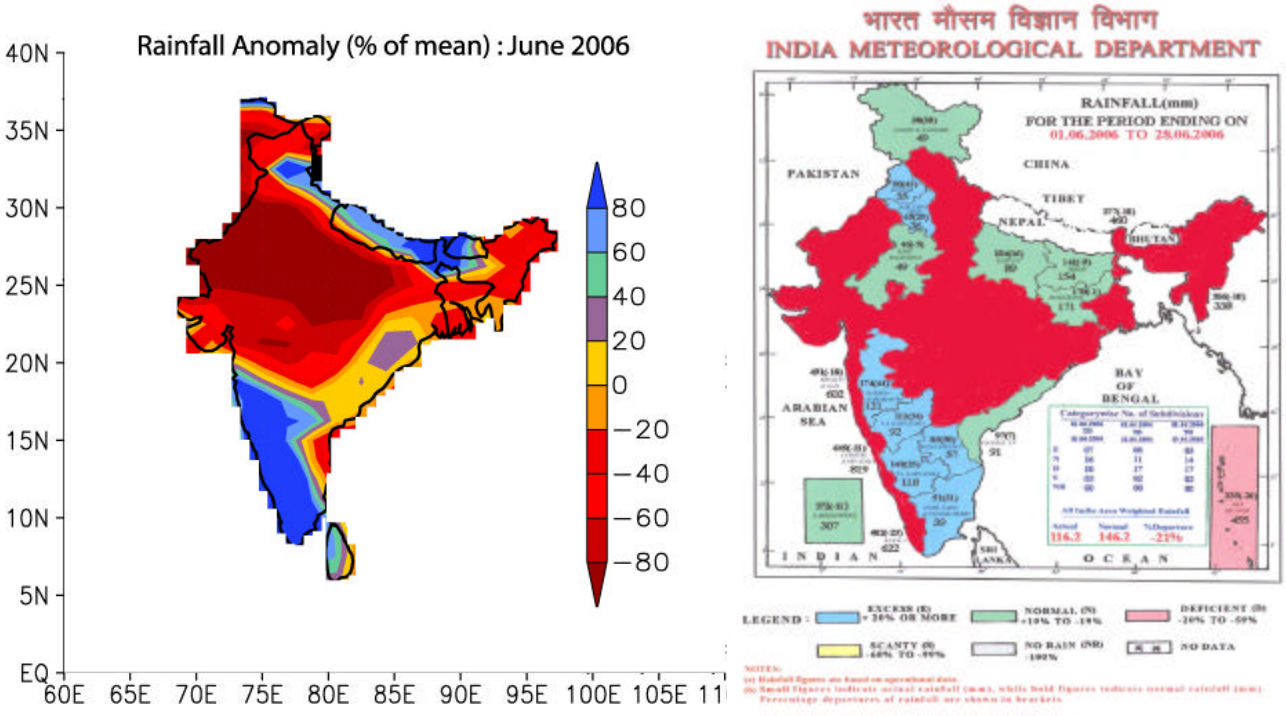

Figure 1.2 Comparison of C-MMACS forecast for June rainfall anomaly with the corresponding observation (www.imd.ernet.in), the areas with less than 10% deficit rainfall in observation have been shaded with red colour in the right panel for ease of comparison.

For a comparison of our forecasts with observation, we reproduce below the highlights of our forecasts that were communicated to the India Meteorological Department (IMD):

1. Marginally deficit (about 5% below model mean) rainfall for continental India as a whole in June, July and August 2006. These deficits are likely to be much higher for central and northern India.

2. Strongly contrasting distribution of rainfall anomalies between southern and the northern India as a whole. While most parts of southern India and the east coast are likely to receive excess rainfall in June, most parts of central India is likely to suffer from severe deficit.

3. Flood-like situation is likely to prevail in Bihar, Jharkhand and West Bengal in July-August, 2006.

Figure 1.3 compares the spatial structures of rainfall forecasts for two weeks with the corresponding observations. Quite predictably, the errors at weekly scale are higher.

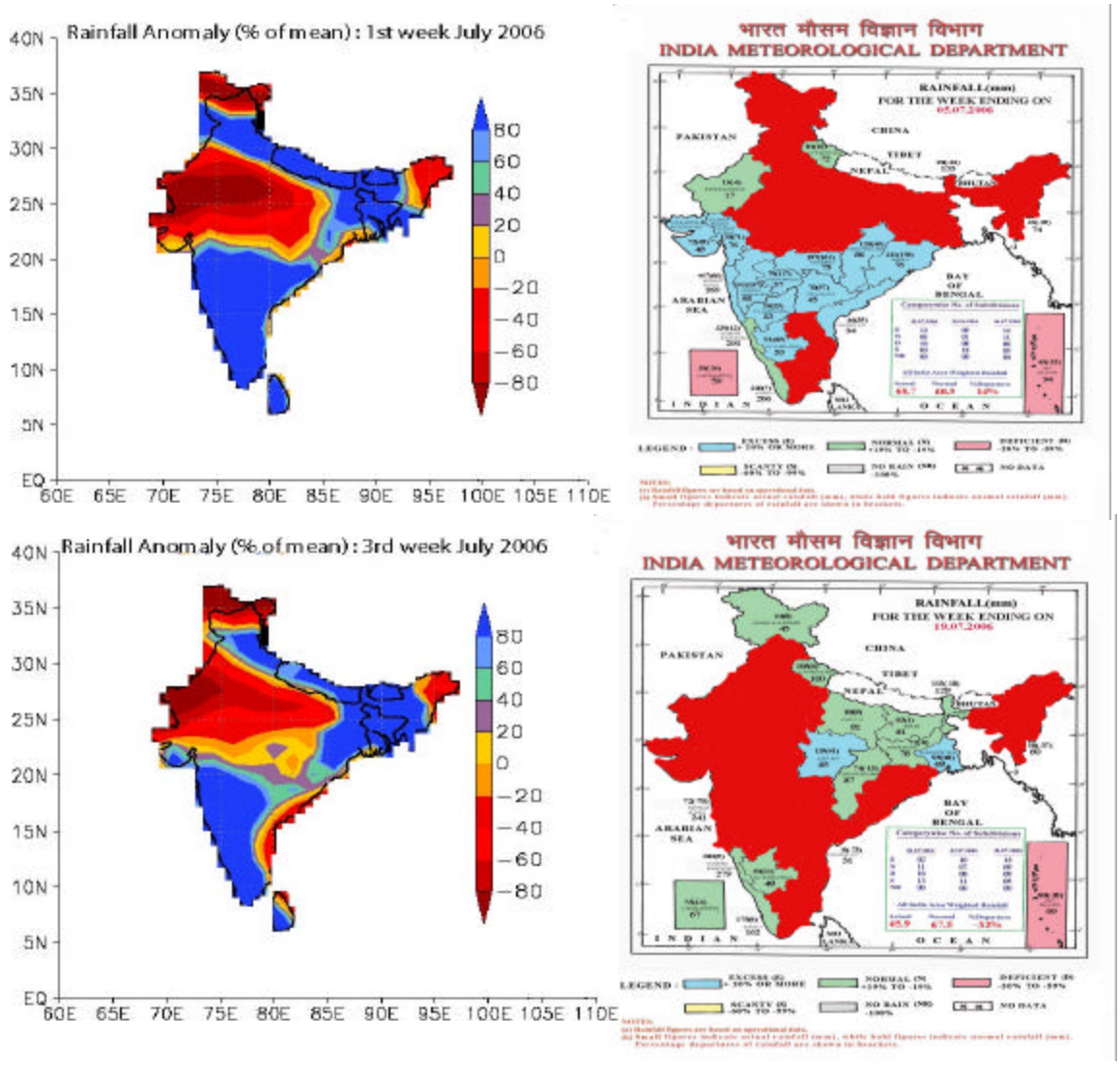

Figure 1.3 Comparison of C-MMACS forecast for two weeks of July (1st week & 3rd week) rainfall anomalies with the corresponding observation (www.imd.ernet.in), the areas with less than 10% deficit rainfall in observation have been shaded with red colour in the right panel for ease of comparison.

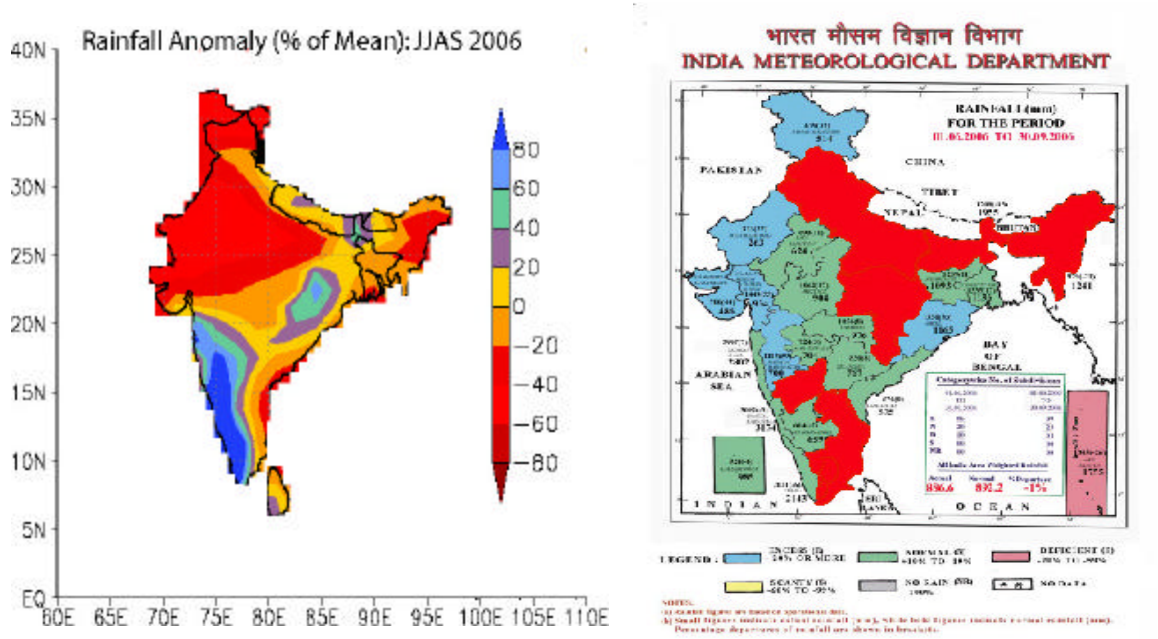

Figure 1.4 Comparison of C-MMACS forecast for seasonal (June-Sept) rainfall anomaly with the corresponding observation (www.imd.ernet.in), the areas with less than 10% deficit rainfall in observation have been shaded with red colour in the right panel for ease of comparison.

A comparison of forecast and observed rainfall for June shows that the forecasts captured many of the observed features. However, although Bihar and Jharkhand recorded normal rainfall compared to deficit rainfall in the neighboring areas, the forecast of flood was wrong. The forecasts did capture, however, the severe drought in the north-east and strong contrast in rainfall in between northern and southern India.

The structure of seasonal (June-September) rainfall from the forecasts is compared with the observed structure in figure 1.4. Once again, this comparison is in the sense of category, so that areas below 10% deficit in observation have been assigned a single color (red). A summary of comparison is as follows:

(a) The main error in the forecast is the large deficit predicted for the north-western sector and Jammu and Kashmir.

(b) The forecasts also over predicted the deficit along the eastern coast.

(c) The forecasts correctly predicted the severe drought over the north-east

(d) The forecasts could capture the excess rainfall over Orissa adjoining areas with severe deficit

(e) The forecasts captured the deficit over the northern belt and eastern India

(f) The forecasts captured the normal to excess rainfall over south-western coast adjoining the deficit area over the east coast.

Given that forecast skill is a complex function of a number of parameters and processes, there is an urgent need to explore attainable skill at different scales; the C-MMACS experimental forecasts are a step in this direction.

K C Gouda and P Goswami

1.2 Onset of Monsoon based on Spatial Coverage

The onset of the Indian summer monsoon (ISM) over Kerala marks the beginning of the main rainy season for India. The onset, however, needs to be carefully distinguished from the synoptic processes that mimic it. The onset of monsoon is a result of a large-scale shift in the regional circulation pattern. In contrast, the so called "false" or "bogus" monsoon onsets are associated with propagating tropical intraseasonal disturbances unrelated to the monsoon onset. These disturbances are characterized by an enhancement of convection and westerly surface winds similar to the monsoon onset but occurring over a smaller scale and lasting a week or less. The false onsets are often followed by extended periods of heat waves and droughts. An incorrect identification of a bogus onset with the date of onset of Monsoon (DOM) can cause considerable economic and agricultural damage, as crops planted in anticipation of the monsoon are likely to fail. The bogus onsets can predate the actual onset by up to a several weeks; thus one of the biggest challenges in identifying, and predicting, date of onset of monsoon is, to avoid these 'bogus' onsets.

Although the onset manifests itself in various dynamical and thermodynamical variables, these can be expected to be closely interrelated and mutually consistent. One index of the large-scale transition in the regional circulation associated with the onset of monsoon is the characteristic change in the rainfall over Kerala. While there exists no unique definition, at the surface the onset is recognized as a rapid, substantial, and sustained increase in rainfall over a large scale; typically, from below 5 to over 15 mm day^{-1} during onset. We have therefore considered only one variable, daily rainfall, to examine its potential to identify DOM as announced by India Meteorological Department (IMD). A feature that characterizes the onset is spatial coherency over a large scale, which is uncharacteristic of synoptic variability. Traditionally, the official announcement of DOM by the India Meteorological Department (IMD) is based on station observations of a number of meteorological variables. Given the tremendous spatio-temporal variability of monsoon rainfall, the effectiveness of isolated station observations in capturing the essential characteristics of the onset process is questionable.

We have quantified and calibrate the large-scale nature of monsoon rainfall in terms of spatial coverage. As shown below, these criteria encompass the conventional criteria for DOM based on rainfall, but have extended scope to avoid bogus onset. Further, these criteria are equally applicable to observed gridded data and model outputs.

Leaving the methodology for obtaining post onset rainfall for a future work, our aim in this work is to formulate and assess such a criterion for determining DOM. The objective criteria adopted by us are thus based on four parameters: pre-onset persistence (PrOP), significance, spatial coverage and post-onset persistence (PoOP). The PrOP and PoOP together ensure that the rainfall observed or predicted is sustained, and not a result of a transitory system. The significance is taken in terms of rainfall above a threshold value, 3 mm/day.

The spatial coverage, above a threshold value, ensures the large-scale, spatially coherent nature of the monsoon rainfall. However, as the traditional announcements of DOM are based on station observations (in Kerala), an appropriate equivalent value for the spatial coverage has to be determined from observed spatial distribution of rainfall. The primary requirement for such an analysis, a high-resolution gridded rainfall dataset, was only recently met with the availability of a 53-year (1951-2003) daily rainfall data on a 1^{o} x

1° grid prepared by the India Meteorological Department (IMD).

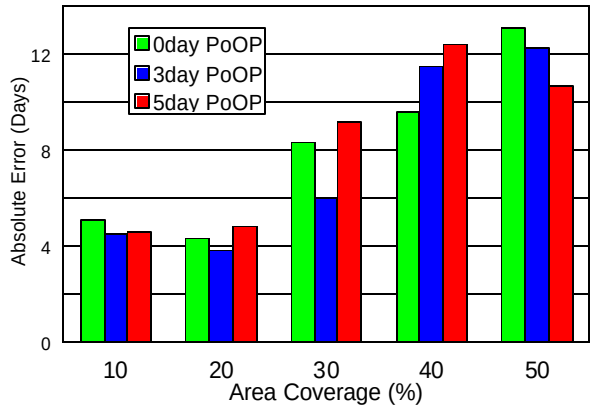

Figure 1.5 53-year (1951-2003) average absolute error in computed DOM for different area coverage. The green, blue and red bars represent, respectively, computed dates based on criteria of 0 (no post-onset persistence), 3 and 5 day post-onset persistence of (threshold) rainfall above 3 mm/day. The Pre-onset persistence is 3 days.

Figure 1.5 calibrates and quantifies the role of spatial coverage in terms of average error in computed DOM for different area coverage (%) beginning 10% and going up to 50 %. An important feature in figure 1.5 is the steep increase in error for coverage (%) beginning 20% of the onset domain. It was found that for area coverage more than 50% a DOM within the May-June period could not be identified for most of the years. The large scale nature of monsoon is thus best reflected in an area coverage of 20% of the onset domain. It was found that for area coverage more than 50% a DOM within the May-June period could not be identified for most of the years.

.

We next evaluate the skill of the methodology in terms of histogram of errors between the predicted dates of onset and the dates of onset computed from the daily gridded rainfall data of IMD following our objective criteria. The hollow, shaded and filled bars in figure 1.6 represent the (% of) cases in different error bins for PoOP of 0, 3 and 5 days, respectively. As can be seen from figure 1.6, both for PoOP of 0 and 3 days, 83% of the cases have error less than one standard deviation, while for PoOP of 5 days this number is 72%. The average error between the announced and computed DOM are 4.3 days, 3.8 days and 4.8 days, respectively, for PoOP of 0, 3 and 5 days, as given in the panel

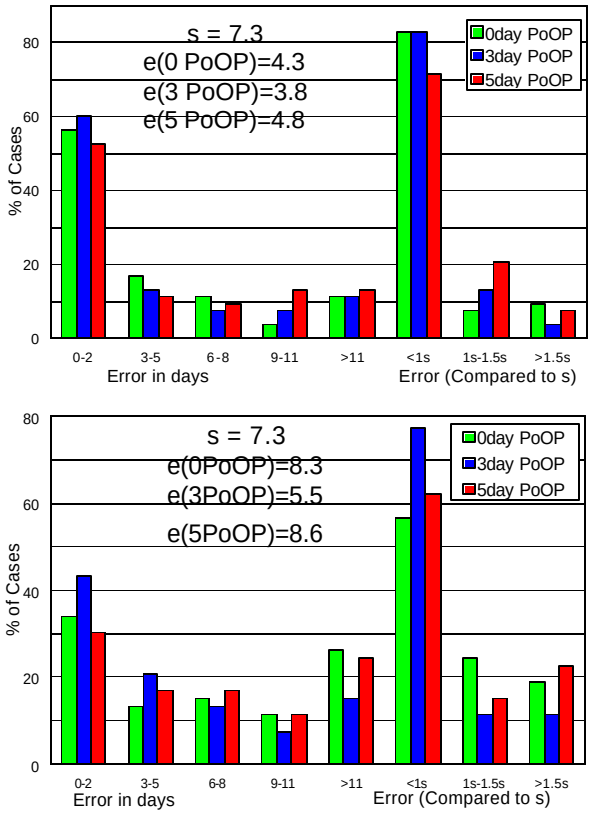

Figure 1.6 Histogram of errors in computed and announced dates of onset with respect to dates of onset computed from daily rainfall data from the India Meteorological department. Both the computed and the predicted dates are based on the criteria of significant rainfall with Pre-onset persistence of 3 days and threshold of 3 mm/day. The hollow, solid and shaded bars represent, respectively, Post-onset persistence of 0 (no post-onset persistence), 3 and 5 days. (a) for the area coverage of 20% over the onset domain (b) for the area coverage of 30% over the onset domain.

It may appear, based on the analysis so far that inclusion of a PoOP doesn't significantly

improve identification of DOM. As mentioned earlier, however, the biggest challenge in identification of DOM is to avoid false onsets. We have therefore compared (Table 1.1) the success of the methodology for seven years that were characterized by false onsets [*Flatau et al.,* 2001] within the period 1951-2003. As can be seen from Table 1.1, the introduction of a PoOP of 3 days considerably reduces error in identification of DOM, the average error for the seven years is only 3.1 days for PoOP of 3 days, as against 7.5 days for no PoOP. Further, with PoOP of 3 days there is only one case of large error (10 days for 1986) as against two large errors (33 days and 10 days for 1972 and 1976, respectively) for no PoOP.

As mentioned earlier the biggest challenge in identification of DOM is to avoid false onsets. We have therefore compared (Table 1.1) the success of the methodology for seven years that were characterized by false onsets within the period 1951-2003. As can be seen from Table 1.1.

	Coverage		
	10%	**20%**	**30%**
1967	3	0	24
1968	0	0	2
1972	33	33	35
1979	0	1	3
1986	6	10	11
1995	5	5	6
1997	4	4	16
Avg	7.2	**7.5**	13.8

Table 1.1 Error in computation of DOM for seven years of false onset with different PoOP and Coverage

It is, of course, neither meaningful nor necessary to insist on a fixed set of criteria to define DOM beyond ensuring its monsoonal characteristics. The traditional definition of the onset of ISM, whether based on rainfall, dynamical fields or hydrological considerations, uses a single set of criteria. However, once these criteria ensure large-scale and sustained nature (that is monsoonal) rainfall, the parameters defining significance and persistence can be process-specific. In practice, it is necessary to consider onset dates based on multiple sets of criteria, as agro-hydrological requirements are likely to be different for different users (such as crop type and catchment's area). Our methodology allows determination of DOM based on such multiple-criteria, as the parameter of emphasis can change from user to user.

Our method thus allows accounting for such parameters like spatial coverage (characteristic of ISM) not possible with isolated station data. Further, gridded data allows a uniform procedure for computing DOM from observations model simulations and other spatial data. While gridded data from IMD observations may not be available on time to be used in determining DOM, remotely sensed data with sufficient spatial coverage provides an exciting possibility. Although model forecasts in principle can be downscaled to station scale, the errors involved are often unacceptable. The use of % coverage largely eliminates errors that may arise from using fixed locations.

K C Gouda and P Goswami

1.3 Optimum Domain Size for Mesoscale Processes Simulation

The most commonly used current strategy for mesoscale simulation and forecasting is Limited Area Models (LAM), three dimensional models with artificial lateral boundary conditions. The methodology adopted in most places in applying these meso-scale models, however, has a serious shortcoming; removable of this weakness is expected to result in better skill, as demonstrated in this work.

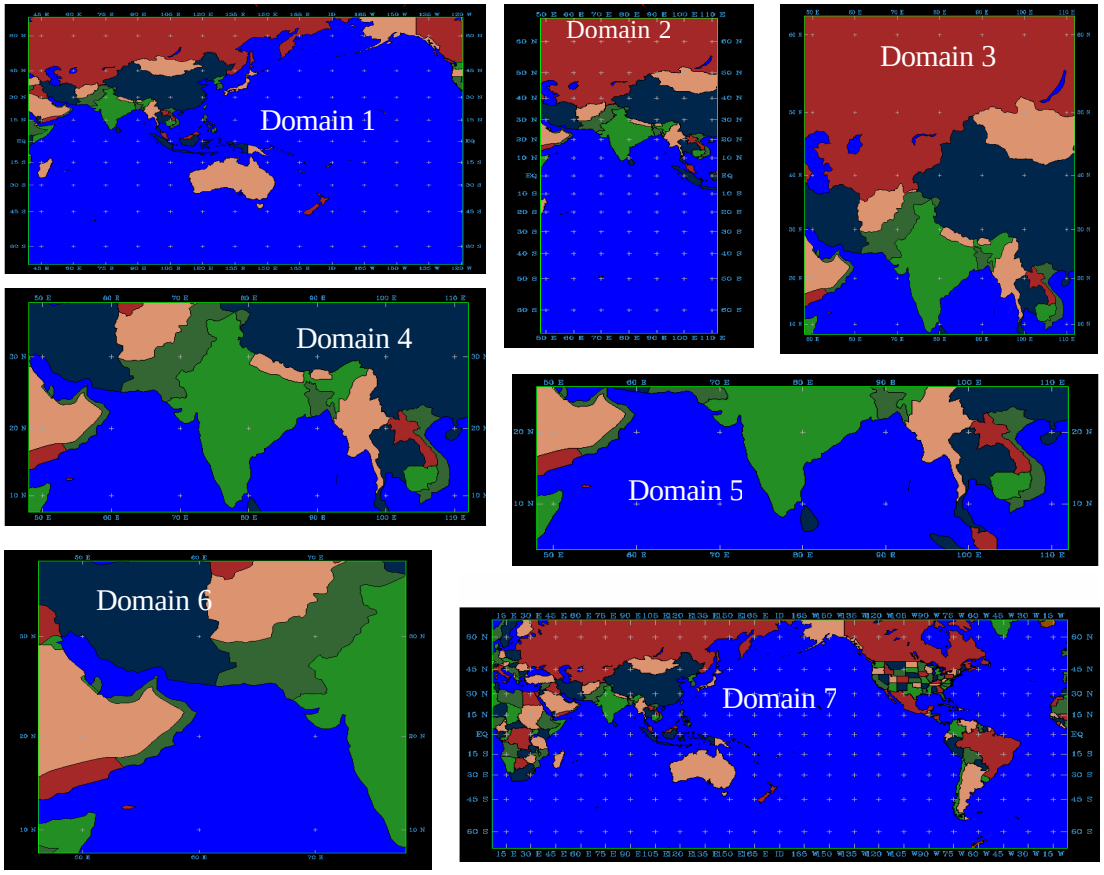

Figure 1.7 Longitudinal and Latitudinal extents and geographical coverage of experimental model domains

While these models can support high horizontal resolution necessary to resolve surface inhomogenities and convective dynamics at scales not yet feasible in General Circulation Models (GCM), a necessary price is the artificial lateral boundaries. The limited domain introduces several aspects to a mesoscale simulation. In particular, there is no unique choice of the extent and geographical coverage of the domain. Besides, the large-scale forcing at the lateral boundaries may not always be dynamically consistent with the inner (mesoscale) fields. The question of the lateral boundary or the domain size is inherently related to model dynamics and physics. While resolution determines the smallest resolved scale, the domain size restricts the largest (horizontal) scale resolved. Thus, domain size and resolution together determine the spectrum of resolved scale and nature of scale interaction in the model dynamics. The geographical coverage (necessarily covering the event location) of the mesoscale simulation domain also plays a significant role by selectively including or excluding processes like orographic lifting and equatorial waves.

We have carried out a detailed investigation of the effect of size and coverage of the domain on the quality of simulation of a mesoscale event. The mesoscale model MM5 was used to investigate the extreme rainfall event that occurred over Mumbai over the west coast of India during 26-27 July, 2005. For each of the five chosen domains (Figure 1.7) with different spatial extent and geographical coverage, simulations were carried out with five initial conditions (leads) for a given resolution with identical physics options. These simulations were repeated for different resolutions (90, 60 and 30km), resulting in a total of 75

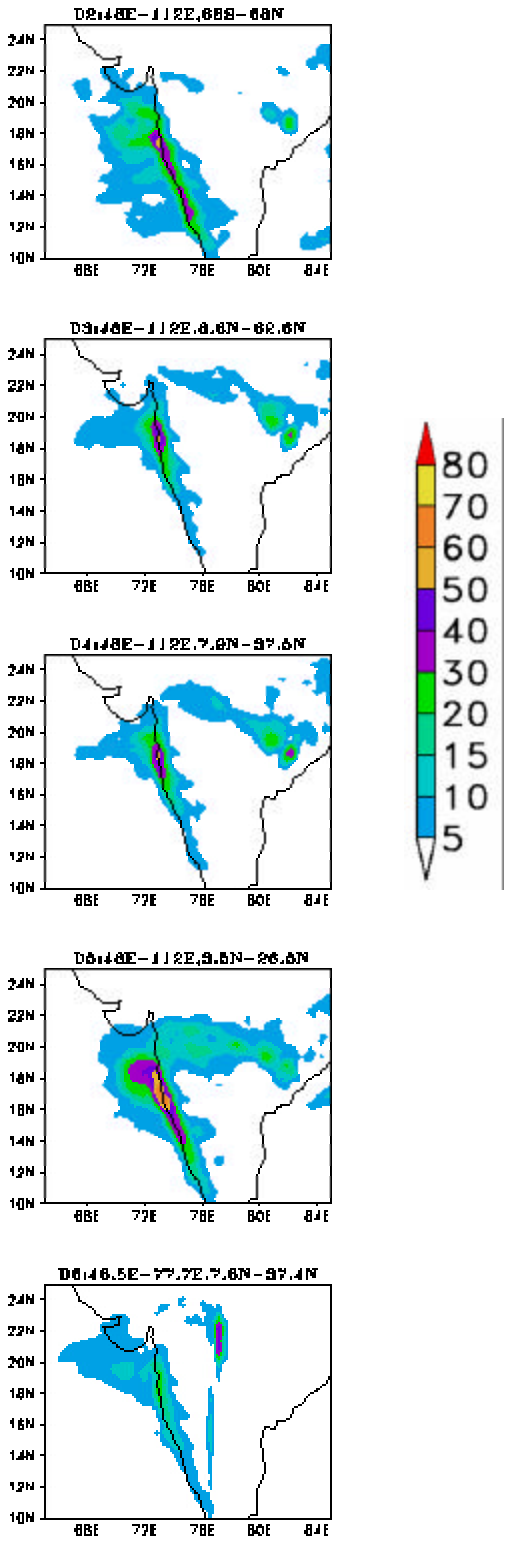

Figure 1.8 Spatial distribution of 30 hour accumulated ensemble mean rainfall for different domains of 30 km resolution.

simulation experiments. In addition, two larger (one nearly global) domains were considered for coarser resolution (90-60km). Our results show that along with resolution, the geographical coverage and the size of the domain also play critical roles in the simulation of a mesoscale event. In terms of (30 hour accumulated) maximum rainfall realized, the domains D1 and D5 resulted in comparable (maximum) values, although the size (area) of domain D5 is much smaller than that of domain D1. Comparative analysis of the results of domain D4 and D5 which are of comparable size is of particular interest. They show significant differences in terms of maximum rain, more so in the case of higher resolution (30 km) compared to 90 and 60 km. The best simulation is found to be for domains that are not the largest but that cover significant part of the equatorial ocean, i.e. domain D5. Lat-Lon distribution of 30 Hr accumulated rainfall for different domains of 30 km resolution is shown in Figure 1.8. Highly localized mesoscale structure may be seen around Mumbai. One possible dynamical mechanism responsible for the influence of domain size can be drawn from a qualitative application of the result (Green's theorem) that a dynamical boundary value problem with inhomogeneous lateral boundary conditions is equivalent to a system with homogeneous lateral boundary conditions with an additional forcing. The inhomogenity in the lateral boundary conditions is thus a measure of variation in large scale forcing with the size and the coverage of the
domains. While this conclusion is likely to change based on event location, our study shows that the choice of the meso-scale domain is a non-trivial but critical input for improved mesoscale simulation and forecasting, and needs to be determined through a comprehensive calibration experiment.

P Goswami and S Himesh

1.4 Extreme Rainfall Events: Vulnerability Analysis for Disaster Management

Extreme rainfall events today pose a serious threat to many populated and urbanized areas worldwide; an accurate estimate of frequency and distribution of these events can significantly aid policy planning and observation system design. We report here a first-ever high-resolution (10 KM) analysis of heavy rainfall episodes (defined as 24-hour rainfall exceeding 250 mm) over the Indian region. The data set, recently developed by National Oceanographic and Atmospheric Administration, USA (NOAA), provides daily composite rainfalls for the period 2001-2006 at locations approximately 10-km apart. To assess the usefulness of the dataset for such application over India, we have compared area-averaged daily rainfall over Kerala (EN) from IMD gridded daily rainfall data and the high-resolution data; Figure 1.9 shows the comparison for these 3 years 2001-03 for which the two data sets overlap. The close resemblance, supported by high-correlation coefficients in spite of inherent uncertainties in creation of gridded data, shows the potential of such an approach. A category-wise analysis identify a number hot spots of vulnerability in terms of annual average number of extreme rainfall events; in particular, the semiarid region in the north-west India emerges a high vulnerability area in terms of extreme rainfall events (Figure 1.9). These findings have important implications for a number of areas like vulnerability assessment and meso-scale forecasting.

The high-resolution analysis also clearly reveals the corridor of the monsoon trough (Continental Tropical Convergence Zone), lined by flower-pot distribution of extreme rainfall events along the flanks (Figure 1.9). The analysis owing to its very high resolution can be also used for precision design of field experiments on the continental trough or on localized extreme events like thunderstorms by optimizing most probable event location and logical constraints.

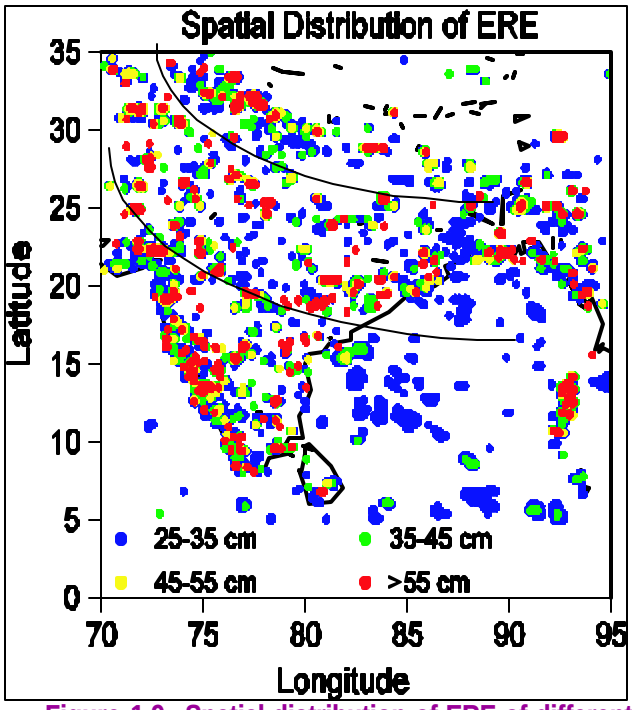

Figure 1.9 Spatial distribution of ERE of different categories accumulated over five years (2001-2005). The high density of ERE over the west coast and along the flanks of the monsoon trough is prominent.

Although the NOAA data set used here allows us much more precise and accurate assessment of spatial and temporal distribution of ERE and thus associated degree of vulnerability, a more comprehensive analysis requires collocated measurements of other dynamical, surface and sub-surface parameters. Based on the precision distribution of the ERE revealed by our analysis, such measurements can be made by placing Automated Weather Stations (meteorological towers) over these locations. Such measurements, supplemented by other observation platforms like remote sensing and upper-air soundings can allow analysis and forecasting of these high-impact events at precision and resolution that can be effective in applications like pro-active disaster management.

K V Ramesh and P Goswami

1.5 Modulation of Tropical Intra-seasonal Oscillations by Coupling: CGCM vs. AGCM Study

Comparison of composite events of Tropical Intraseasonal Oscillations (TISOs) [(i) eastward propagating Madden-Julian oscillation (MJO) during Boreal winter and (ii) northward propagating intraseasonal oscillation (NPISO) during Boreal summer] constructed based on objective criteria, shows that the three dimensional structure, amplitude and speed of propagation, and the phase relationship among surface fluxes, sea surface temperature (SST) and convection, are markedly improved in a coupled GCM (CGCM) simulation compared to its stand alone atmospheric GCM (AGCM) forced with CGCM SSTs. Consistent with the frictional wave-CISK (Conditional Instability of the Second Kind) mechanism, successive development of low-level convergence to the east (north) of deep convection was found to be important for eastward (northward) propagation of MJO (NPISO). For example, Figure 1.10 shows that in contrast to AGCM simulation, the composite NPISO event evolves as a strong coupled mode in CGCM as in observation. The simulated NPISOs in its atmosphere-alone component lack many of the important features not only associated with their amplitude, phase and life-cycle but a coherent coupled feedback process as well.

The phase relationship between rainfall (PR) and SST, wind stress (t), fluxes of SH, LH, SW_{Net} , Q_{Net} , LW_{Net}, moisture divergence (M) and divergence (D) at 200 hPa and 925 hPa at the reference point 15N; 90E during a TISO composite is shown in Figure 1.11. Net fluxes (SH, LH) are positive into (out of) the ocean. Symbols '+' indicate maxima and '-' indicate minima of the correlations. In CGCM, coherent coupled convective-thermodynamic feedback is evident from the strong correlations and their temporal evolution in the coupled model through the full half cycle. In contrast, the AGCM shows weak and insignificant lag correlations during the SST half cycle. Due to the absence of direct interaction of convection and surface fluxes in modulating SST, there is a complete breakdown of the coherent evolution of the phase relationships except for warm SST boundary anomalies directly modifying the large-scale dynamical fields and causing the precipitation. This conveys that a realistic representation of the interaction between sea surface and the atmospheric boundary layer is crucial for the simulation of TISOs.

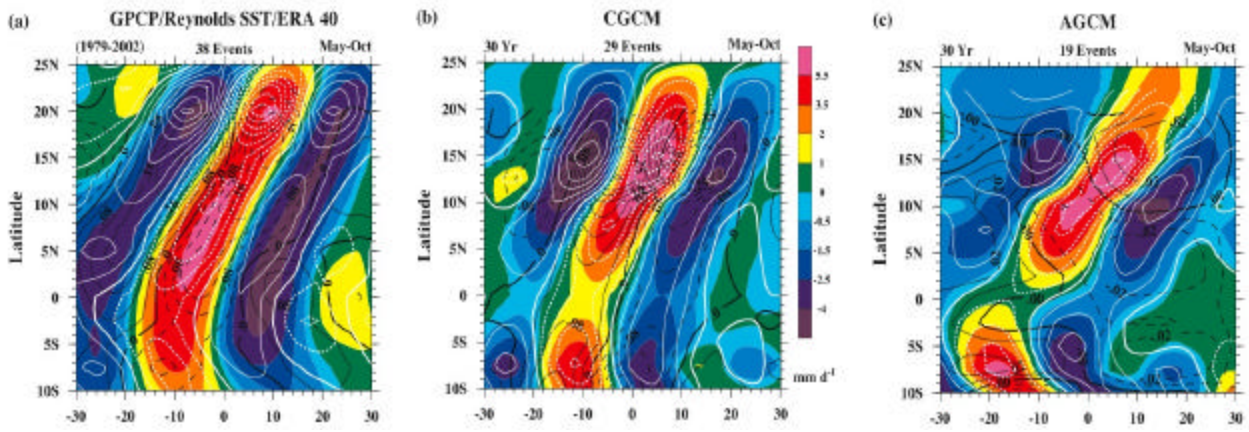

Figure. 1.10 Latitude vs. lag diagram of composite anomalies of rainfall (shaded), SST (black contours) and 925 hPa divergence (X10^6) (white contours at 0.4 interval) at 90E. Number of events are 38, 29 and 19 for observation, CGCM and AGCM respectively.

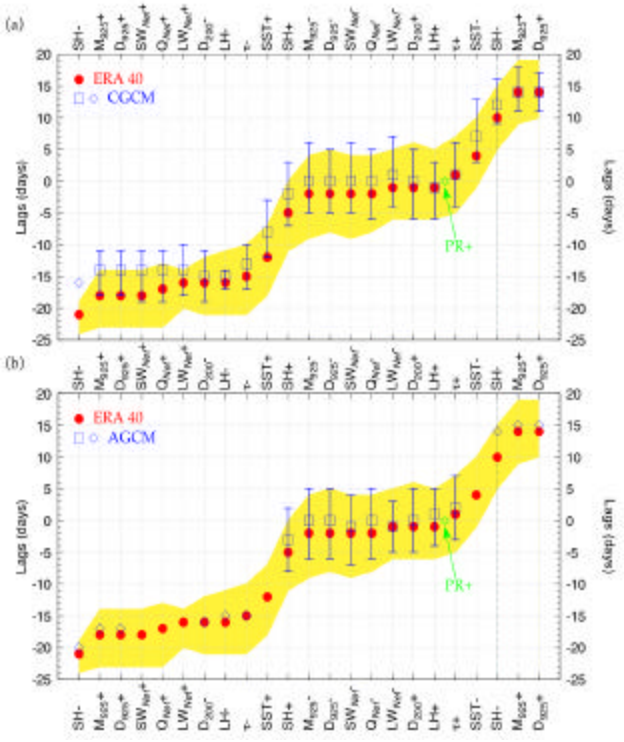

Figure 1.11 The temporal relationships for the (a) CGCM and (b) AGCM simulations are shown against the corresponding observation in the background. The filled circle indicate the lags at which the correlation maxima (minima) which are above (below) the 95% significance level occur for each variable from observation and the shades indicate the corresponding lag range of 95% levels . The box (diamond) indicates the lags at which the correlation are significant (insignificant) at 95% level for the simulations and the solid bars indicate their corresponding lag range for 95% levels.

K. Rajendran and A. Kitoh

1.6 Western North Pacific Circulation Modes and Tropical Cyclone Landfall in Japan

Large-scale seasonal circulation during June-October over western North Pacific shows two dominant modes; the El Nino Southern Oscillation (ENSO) mode and a mode correlated with the variation of the subtropical high (STH). The second mode of CEOF (Combined EOF) analysis for vertically integrated lower tropospheric zonal and meridional winds (Ui, Vi), geopotential height at 850 hPa (Z850) from ERA-40 reanalysis and the temporal variation associated with this mode is shown in Figure 1.12. The horizontal fields of Ui, Vi and Z850 show that there are two centers of action, one is a low-pressure anomaly centered near 20 °N, 135 °E and the other is a high-pressure anomaly centered near 40 °N, 160 °E. In its positive phase, the equatorial westerly anomalies enhance along 10°N over the western North Pacific and the STH retreats eastward.

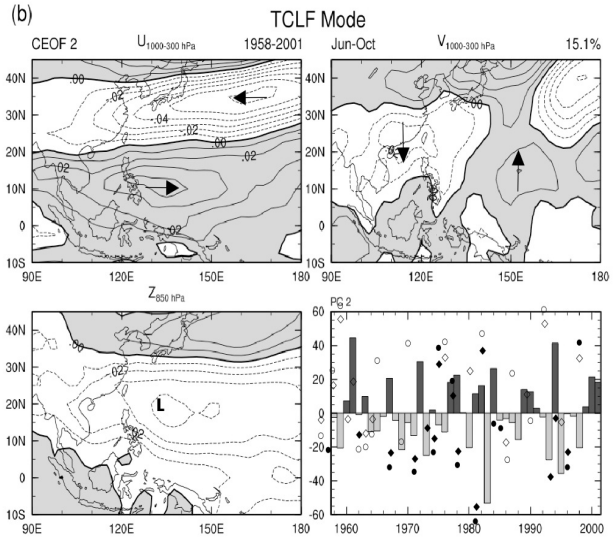

FIG 1.12 The second mode of the CEOF for Ui, Vi and Z850 from ERA-40. Shaded contours denote positive values. TC+ (TC-) denotes years with more (less) number of tropical cyclone landfall. CG+ (CG-) denotes years with more (less) number of tropical cyclone genesis. The open (solid) rectangles and circles denote TC+ (TC-) and CG+ (CG-) years. "L" in Z850 (bottom-left) represents the centre of the anomalous low pressure.

In contrast, during its negative phase, the equatorial easterly anomalies enhance over the region to strengthen the climatological easterlies and thus extending the STH westward. The extensive analysis of long-period data revealed that in years when the STH extends westwards from its climatological position and the maximum of the high pressure anomaly is located along the Tropic of Cancer, the frequency of Tropical Cyclone (TC) approach or landfall in

Japan tends to be reduced. It is partly due to less number of TC genesis (CG-) over the western North Pacific in these years. In contrary, when the STH retreats eastwards and the maximum of the low pressure aomaly is located along the Tropic of Cancer, there is a tendency to have more number of TCs approach or make landfall (TC+) in Japan. Based on these results, this mode is named as the tropical cyclone landfall (TCLF) mode.

T. Nakazawa and K. Rajedran

1.7 Ensemble simulation of Indian Summer Monsoon Rainfall by an AGCM

The simple ensemble mean (SEM) of the AGCM forced with observed monthly mean SSTs starting from different initial conditions shows systematic bias in simulated climatological ISMR pattern and mean seasonal variation of rainfall over the Asia-Pacic region. Concurrently, the monsoon interannual variability throughout the analysis period is not adequately represented. A bias-correction method is applied to the member simulations to remove the systematic bias in the simulation of climatological features. This method derives correction coefcients for the members for each Julian day separately at every grid point through multiple linear regression of daily rainfall from the member simulations against corresponding observation over a long training period. Thereafter, at every grid point, for each Julian day of any forecast period, the bias removed ensemble mean (BREM) simulation is computed as an optimal linear combination of weighted member simulations. It is found that BREM improves upon SEM not only in simulating the mean ISMR pattern but also in capturing the interannual variability of ISMR during the entire analysis period. In addition, the effective removal of climatological bias in BREM also improves its subseasonal evolution (during 2002 monsoon season is shown in Figure 1.13) particularly associated

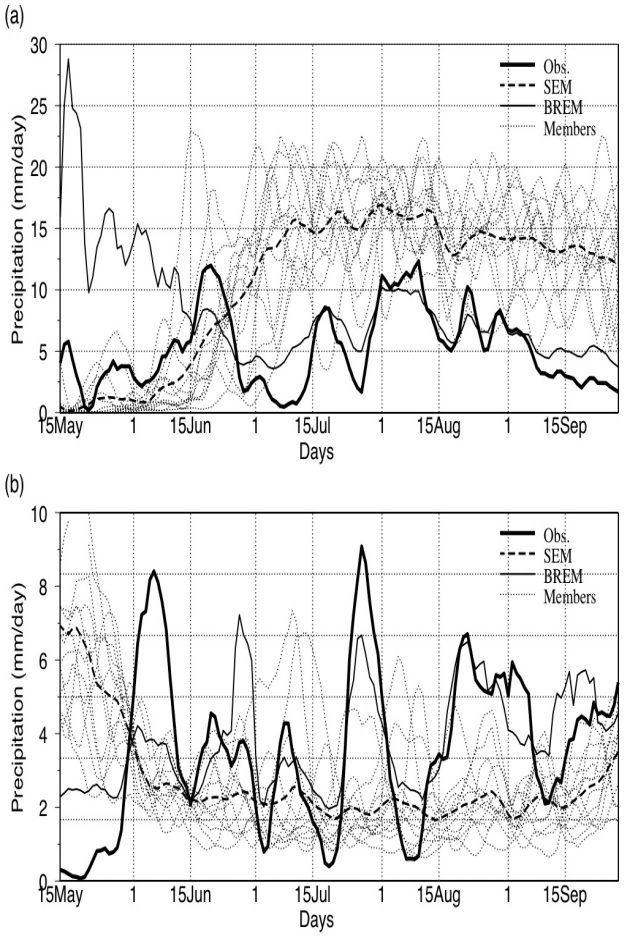

Figure 1.13 5-day running mean applied daily rainfall averaged over (a) continental central India and (b) equatorial Indian Ocean from observation, members, SEM and BREM simulations.

with the low-frequency intraseasonal variability. The analysis thereby underlines the importance of climatological seasonal variation of rainfall over the Asia-Pacic region not only for capturing interannual variation of ISMR and climatological ISMR pattern but also for improving its intraseasonal variability.

S Sajani, T Nakazawa, A Kitoh and K Rajedran

1.8 The role of low-frequency intra-seasonal Oscillations in Anomalous Indian Monsoons

Low-frequency intraseasonal time scales in?uences the nature of onset, intensity and duration of active/break phases and

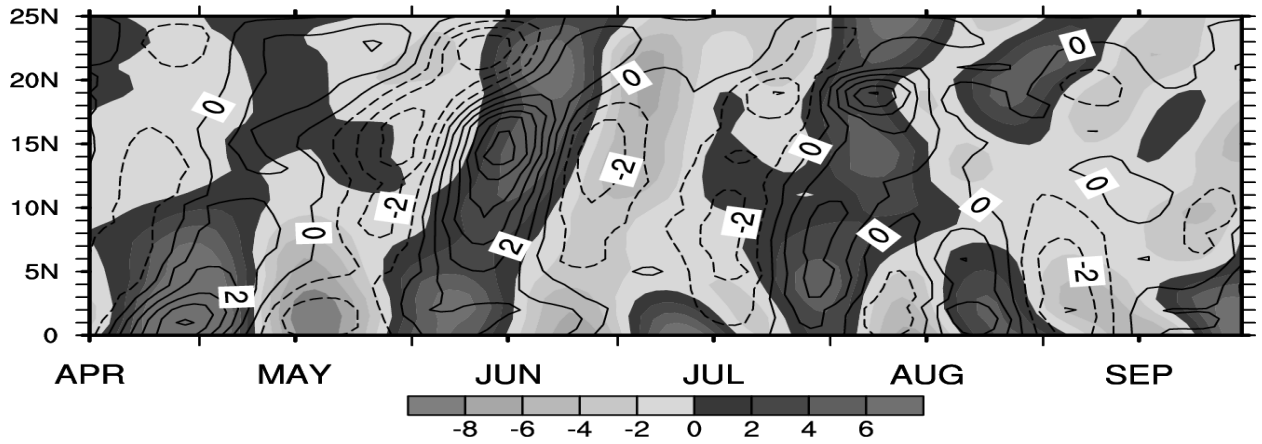

Figure 1.14 Time-latitude variation of 20-80 day filtered observed rainfall averaged over 75E-85E (shaded) and corresponding filtered anomalies of surface wind over the Arabian Sea (contours).

withdrawal of the monsoon during anomalous Indian summer monsoon seasons. For example, during the most severe drought of 2002, persistent warm sea surface temperature anomalies over the equatorial Indian Ocean played a signi?cant role in modulating the strength of the monsoon Hadley circulation. This in turn affected the onset and intense break spells especially the long break during the peak monsoon month of July. Further, SST anomalies over the equatorial Indo-Paci?c region on low-frequency intraseasonal time scales were found to a? ect the equatorial eastward and thereby off-equatorial northward propagations (shown in Figure 1.14) of enhanced convection over the Indian region. These propagations in turn modulated the active/break cycle deciding the consequent severity of the 2002 drought.

S Sajani, S Naseema Beegum, K Krishna Moorthy

1.9 Mathematical Modelling of Biogeochemical Cycles in the Indian Ocean

The main objectives in biogeochemical modelling studies are identification of key biogeochemical elements/compartments and processes, estimation of the model parameters and evaluation of the integrated system models through model-data comparison at different temporal scales. We examine the effect of five relations governing the uptake of nitrate and ammonium by phytoplankton on the state variables of a seven-component ecosystem model in the 1-D physical framework given in the Arabian Sea Testbed. This marine ecosystem model is evaluated by using US JGOFS data and buoy data at S7 (15.5°N, 61.5°E) in Arabian Sea. The seasonal variations of depth integrated values of primary productivity and chlorophyll are compared with the buoy data during 1994-95. Observed column-integrated primary productivity (PP) and chlorophyll (Chl) (Figure 1.15**)** suggest two highly productive seasons, namely, December to March (North East Monsoon and boreal winter) and July to October (South West Monsoon). Each season has two major and one minor bloom. The modeled PP and Chl show a similar tendency towards greater productivity in these seasons, but with more blooms of shorter duration.

While this investigation did not clearly identify the most appropriate model of nitrogen kinetics, it showed that modeling of nitrification is essential in an ecosystem model. Two numerical simulations were carried out by introducing the nitrification process in the ecosystem model with YS relation for nitrogen kinetics, to test whether

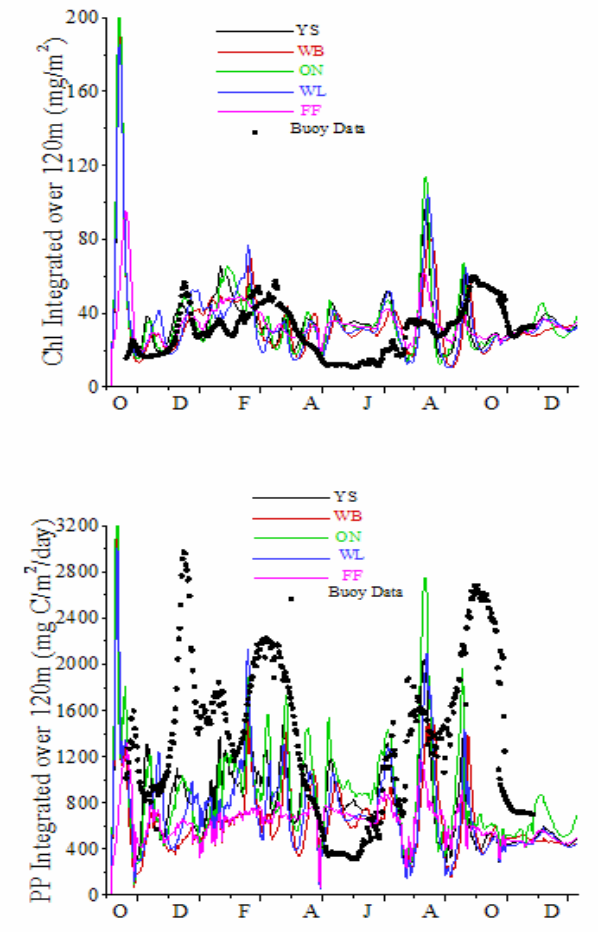

Figure 1.15 a Seasonal variation of Depth Integrated Primary Productivity (mg C/m2/day) compared with Buoy Data Figure.b Seasonal variation of Depth Integrated Chlorophyll (mg Chl/m2) compared with Buoy Data

incomplete modeling of remineralisation was responsible for some of the differences. Seasonal variation of Nitrate and Ammonium in upper ocean (Figure 1.16 and 1.17) shows that nitrification reduces the concentration of ammonium and increases nitrate throughout the water column in all seasons.

Parameter sensitivity studies are done using a 3D coupled physical-biological-chemical model. The marine ecosystem model is evaluated by using US JGOFS data, BOBPS data, satellite data and buoy data for different values of a few of the parameters which influence the regeneration of ammonium and

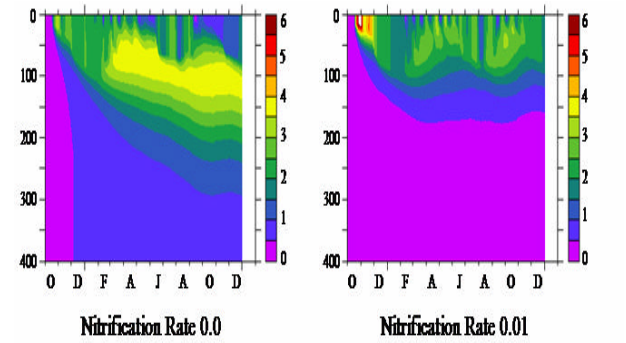

Fig.3 Seasonal variation of Ammonium (Nr - mMolN/m^3) during 1994-95 with depth for three model simulations with YS nitrogen kinetics, with nitrification rates 0, 0.01 and 0.03/day

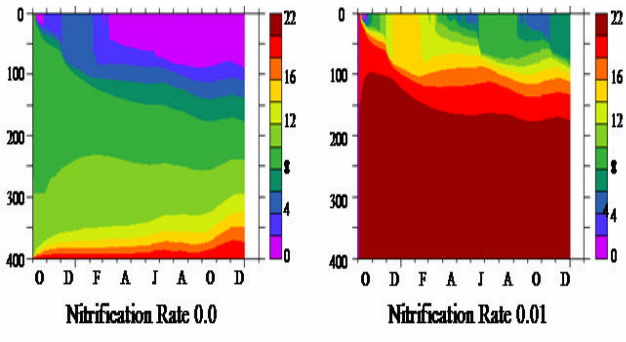

Fig.2 Seasonal variation of Nitrate (Nn – mMolN/m^3) during 1994-95 with depth for three model simulations with YS nitrogen kinetics, with nitrification rates 0, 0.01 and 0.03/day

growth of zooplankton and hence the carbon flux across the air-sea interface. The basin-wide variations of primary productivity (PP) in the euphotic zone and surface chlorophyll (Chl) obtained from simulations agree well with the SeaWiFS data except in regions of

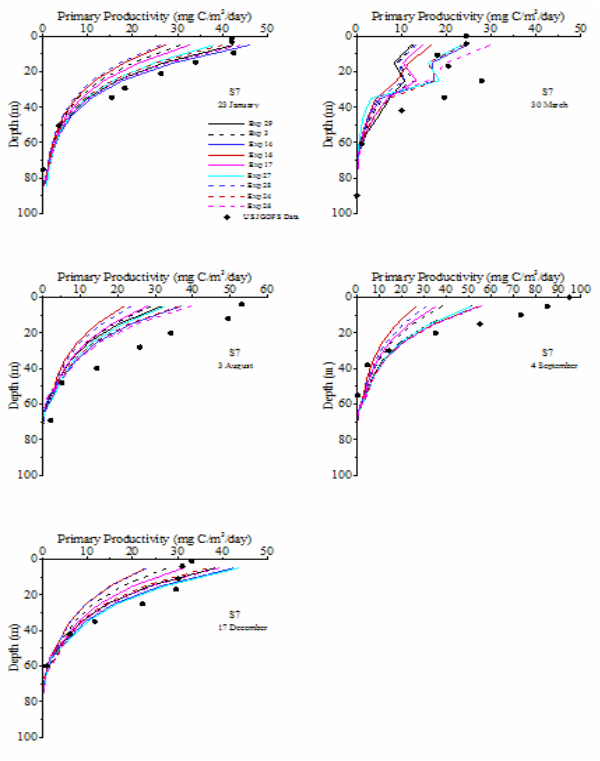

Figure 1.18 Profiles of PP (mg C/m3/day) obtained from nine numerical simulations compared with US JGOFS cruise data during five times over a year at S7 (15.5° N, 61.5° E) in AS.

freshwater input from rivers, for all seasons. The profiles of Chl, PP, Zooplankton (Z), Bacteria (B), Nitrate (Nn) obtained from nine numerical experiments are compared with the cruise data from US JGOFS at four stations in AS and with BOBPS data at two stations in BOB during different seasons. Figure 1.18 shows the comparison of PP obtained from nine model simulations with US JGOFS data at a stationin central AS. Minimum values of PP are obtained when some of the parameters are changed to reduce the regeneration of ammonium by zooplankton. Depth integrated values of Chl, PP, Z and Bacterial production are compared with the cruise data in Arabian Sea. It is noticed that maximum values of zooplankton biomass are obtained for the simulations when grazing rate is reduced or half-saturation constant is increased. Nitrate concentrations obtained from the numerical simulations where regeneration of ammonium by zooplankton is reduced, are closer to observations. Spatial variation of new and regenerated production shows that regenerated production is higher than new production for all numerical experiments.

P S Swathi, M K Sharada, K S Yajnik and C Kalyani Devsena

1.10 Climate Impact of Regional Aerosols over India: An AGCM study.

A global GCM was used to carry out climate sensitivity to aerosol characteristics making use of the large observational database of regional aerosols being generated under the Aerosol Climatology and Effects (ACE) project of ISRO-GBP.

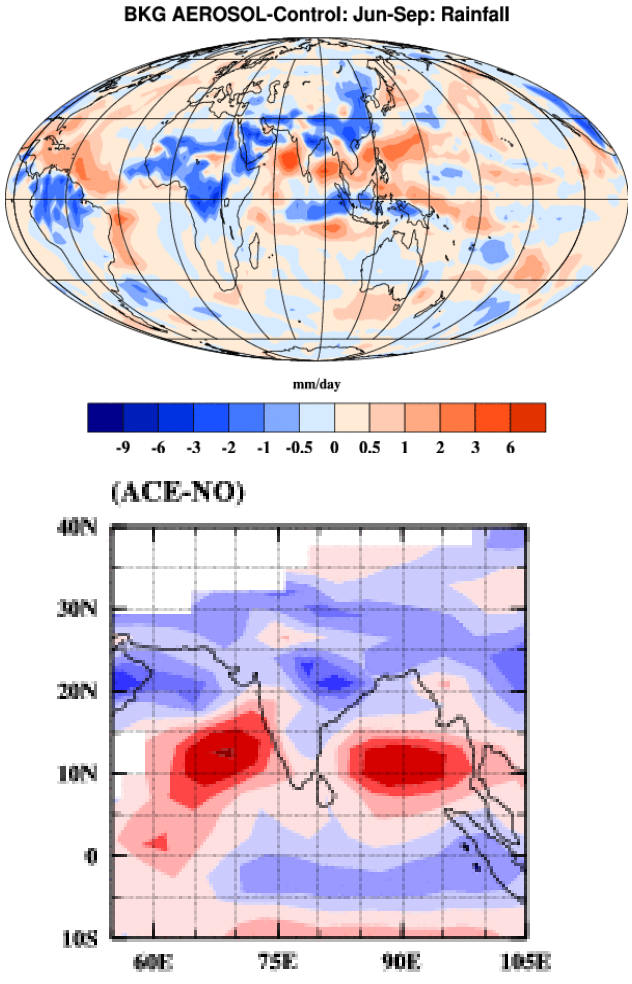

Figure 1.19 Aerosol climate sensitivity in global (top) and regional (bottom) seasonal mean rainfall.

Global Boreal summer mean precipitation shows large climate sensitivity to a blanket distribution of background aerosol optical depth (AOD) of 0.15 (referred to as 'BKG' in top panel of Figure 1.19). Introduction of realistic AOD values from ACE network observations over India (referred to as 'ACE') shows that large quantitative and to some extent qualitative differences in simulated regional climate depending on the changes in aerosol representation in the model (e.g.,climatological summer rainfall difference between ACE and no-aerosol run of the model in bottom panel of Figure1.19). This indicates the improtance of incorporation of realistic AOD values to assess the simulated climate and climate projections using GCMs.

S Sajani, K Rajedran, and K. Krishna Moorthy

1.11 Carbon Fluxes in India and Central Asia (CaFICA): Network Design

In collaboration with Dr. Peter Rayner after the discussion meeting and workshop in Nov/Dec. 2006 on the network design using the output from MOZART a study was initiated to design a network to minimise the trace of the a-posteriori covariance matrix of errors in sources using the genetic algorithm as outlined below.

The focus in the first phase of this study is on Transcom regions (11 land and 11 ocean covering the entire globe) for source/sink determination and seasonal inversion (also called cyclo-stationary inversion). The forward runs for transport involved the use of 4 background tracers (fossil fuel 90 and 95, net ecosystem productivity and oceanic uptake) and 264 pulsed tracers (a monthly pulse from each region) tracked for 3 years following the pulse. The forward runs were made with MOZART, a state of the art transport model with T42 resolution using repeating 1996 NCEP winds. The monthly mean signals from all the runs (at each grid point for 36 months; nearly 10 GB of output) at each grid point was archived.

In the seasonal inversion, for a given network of stations, signals were extracted at each of these stations (closest grid point) and reduced to a seasonal signal to be compatible with seasonal observations. For a linear inversion set-up of GS=D, where G is the model matrix, S is the source/sink estimate to de determined and D is the data vector, the Bayesian approach of inversion minimizes the following cost function:

$$(S-S_0)C(S_0)^{-1}(S-S_0)^T+(GS-D)C(D)^{-1}(GS-D)^T \qquad (1)$$

where C(S0) and C(S) is the a-priori and a-posteriori estimates of source errors. The values of C(S0) are taken from the Transcom TDI protocol.

The posteriori estimate of source errors is given by

$$C(S)=(G^TC(D)^{-1}G+C(S_0)^{-1}) \qquad (2)$$

The metric we use for the “goodness” of a network is the trace of C(S) matrix. In the network design, we aim to find a network of stations that minimizes this quantity. Notice that C(S) depends only on G, C(S0) and C(D) and does not depend upon the D vector.

Genetic Algorithm (GA) is used to determine the optimal network of stations. The algorithm maintains a population of potential networks (200 in this case) chosen at random. Each network has 50 stations (also called parameters). For each of the stations in each network, a data error of 1 ppm (diagonal entries) of the C(D) matrix is assigned. The G matrix for each network is built from the full 3-D transport simulations of MOZART. The TDI inversion (the solution to Eq. 1) is applied to each of the networks and the trace of the C(S) matrix (Eq. 2) is computed for its fitness (or goodness). In the iterative step of the algorithm, members of the population will exchange parameter values pairwise (cross-over), have parameter values randomly changed (mutation), be culled according to its fitness, be cloned or

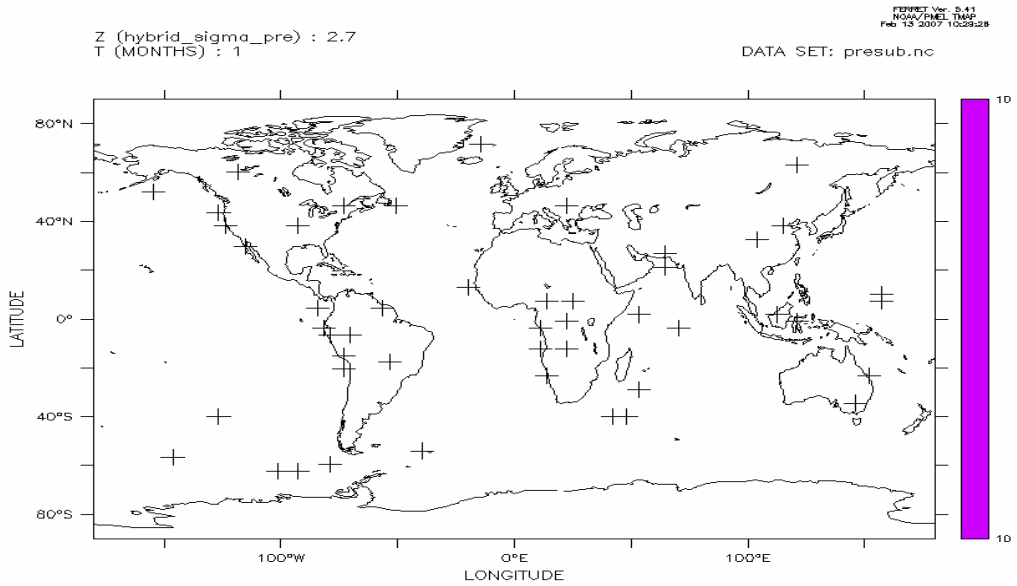

Figure 1.20 The 50 station optimum network is shown .

otherwise reproduce to rebuild the population after culling.

The above four steps constitute one step of the GA. After these, we again build the G matrices and perform the TDI inversion and repeat the iterative steps of GA.

Notice the preponderance of stations in the tropics, especially, in South America and Africa. These are regions of large prior uncertainties in sources (see below) and GA tries to minimise these by adding more stations in these regions. The prior uncertainties (C(S0)) and the uncertainties of the optimum network are given below:

REG	LND_PR	OCEAN_OPT	LND_PR	OCEAN_PR
1	0.495 (Bor Namer)	5.595 (NPac)	21.4	31.6
2	0.991 (Temp Namer)	8.745 (Eq EPac)	116.4	12.2
3	2.071 (Trop Amer)	4.548 (Eq WPac)	258.8	15.1
4	1.880 (S Amer)	5.176 (S Pac)	114.1	71.2
5	1.197 (N Africa)	1.235 (N Ocn)	86.4	3.0
6	1.995 (S Africa)	4.214 (N Atl)	126.3	7.4
7	1.659 (Bor Asia)	4.548 (Eq. Atl)	86.6	7.4
8	2.004 (Temp Asia)	2.711 (S Atl)	96.4	10.9
9	0.750 (Trop Asia)	4.529 (S Ocn)	52.6	108.0
10	0.959 (Aus NZ)	7.705 (N Ind)	15.0	26.4
11	1.326 (Eur)	6.444 (S Ind)	81.1	14.3

In addition, the Southern Ocean which had a large prior uncertainty has 5 stations. Some regions like Europe, Australia and Boreal Asia get only one station each. The total uncertainty for the prior is 1360 (GTC/yr)^2 while the optimum network is 70 (GTC/yr)^2.

P S Swathi, N K Indira, PJ Rayner and V K Gaur

1.12 Establishment of the Flask Station in Pondicherry

A new flask station for collection of CO2 samples has been established in Pondicherry University campus in Sep. 2006. The site was chosen on account of its location on east coast of India and its ability to sample clean oceanic air from the Bay of Bengal and the Indian Ocean. From an initial sampling rate of once in 10 days, the present sample is collected once a week. The collection point is at the top of a 5 m tower on the roof of PU Guest House building. The fist set of samples have been sent to LSCE, France for analysis.

Figure 1.21 A view of the collection site, collection unit and an automatic weather station set up near the measurement site.

N K Indira, P S Swathi, B C Bhatt, V Reddy, V K Gaur and M Ramonet

1.13 The Expanding Indian Desert: Assessment Through Weighted Epochal Trend Ensemble

One of the biggest challenges in climate research is to arrive at reliable future projections. However, while there now exists a firm scientific basis and procedure for climate forecasts, numerical climate models still suffer from large uncertainties. Observed local trends do reflect combined effect of both anthropogenic forcings and natural variability over a location; however, projections based on a linear trend may have considerable error as the trends are generally significantly non-linear owing to low frequency natural variability and the resultant changes (second derivatives) in the trends. In this work we adopt a weighted epochal trend ensemble (WETE) approach to assess the stability of the Indian desert with increased reliability. Ensemble techniques have generally helped to reduce uncertainties in forecasts and the weighted epochal trend ensemble proposed here takes into account the inherent non-linearity in the trend by considering a piece (epoch)-wise linear trend and its weighted contributions to construct more reliable future projections of local climate change. Both the WETE and Linear projections of desert area over India based on annual rainfall and show that the Thar Desert in western India is expanding in a north-east direction. Both the simple linear trend and the epochal trend ensemble projections indicate significant increase in the desert area over India over the next hundred years; however, there are also significant differences between the two projections. An index of aridification can be defined as the number of grid points (percentage of total area) that receives annual rainfall less than or equal to the annual mean rainfall over Thar (258 mm) desert in a persistent manner. Both simple linear trend and WETE projections show **(**figure 1.22) a steady increase in the desert coverage over India for the next hundred years. However, there are also differences between the two projections. Both the projections show that the percentage area covered by desert

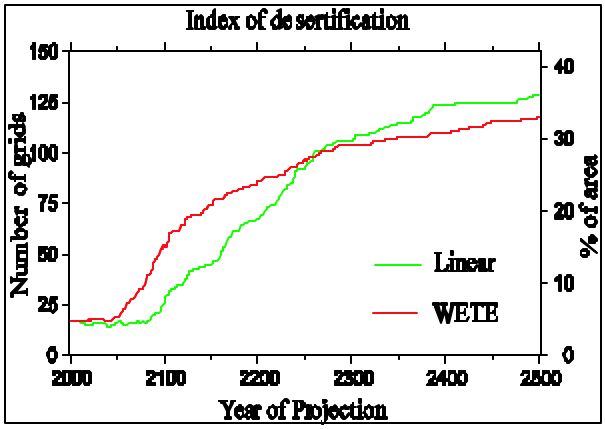

Figure 1.22 Index of desertification in terms of percentage of number of grid points (left axis) and percentage of total area (right axis) during the period 2000- 2500 based on observed rainfall over last 53 years. The projection based on 53-year simple linear trend shows no significant desertification for the next hundred years, followed by rapid desertification that saturates at about 35% (as against the current 23%) of the total area around 400 years (around the year 2400). In contrast, the WETE projection (red line) shows rapid desertification that begins after about 50 years (around the year 2050) that saturates at about 32 % of the total area around the year 2200

conditions is going to increase rapidly, and then remain steady at that level for the next five hundred years. However, while the desertification increases only after hundred years in the linear trend projection, the WETE projection shows a steep increase starting about fifty years from now. In view of our earlier assessment of the reliability of the two projections, we can assume that a sharp rise in desertification is likely to begin about fifty years from now, although both the projections predict saturation at about 30-35% of the total area after about 300 years from now. The results of the validation are used to choose the more reliable projection, which shows a sharp increase in the size of the Indian desert in the next hundred years.

P Goswami and K V Ramesh